



Monte Carlo Based Dose Assessment for ⁹⁰Y Radioembolization, A Comparison between ^{99m}Tc-MAA SPECT/CT and ⁹⁰Y-Microspheres PET

Sjoerd Rijnsdorp¹, Daniela Oprea Lager², Jan de Vries³, Arthur van Lingen⁴

Department of Medical Physics, Catharina Hospital, Netherlands¹

Department of Radiology & Nuclear Medicine, VU University Medical Center, Netherlands^{2,3,4}

Abstract

The aim of this research was to assess the agreement between the distribution of technetium-99m macroaggregated albumin (MAA) and yttrium-90 microspheres in radioembolization of the liver, as well as the correspondence between the desired radiation dose and the true radiation dose in the target area.

Materials and Methods: The relative distribution of yttrium-90 microspheres was estimated in 5 patients, using the activity distributions from technetium-99m MAA SPECT/CT and yttrium-90 PET/CT imaging.

A Monte Carlo simulation using these relative activity distributions was used to calculate the radiation dose to the liver.

Results and Discussion: A large difference in radiation dose was found when comparing technetium-99m MAA and yttrium-90 microspheres distributions. In addition, the distribution of yttrium-90 microspheres in the liver, obtained from the PET images, was highly inhomogeneous.

Relative technetium-99m MAA distribution does not necessarily comply with the distribution of yttrium-90 microspheres. Therefore, technetium-99m MAA scans cannot directly be used for prospective radiation dose assessment. Due to the inhomogeneity of the distribution of yttrium-90 microspheres, the estimated radiation dose in large parts of the targeted lobe(s) is smaller than the desired radiation dose.

Keywords: Radioembolization, Yttrium-90 Microspheres, Technetium-99m Macroaggregated Albumin, Hepatocellular Carcinoma, Single Photon Emission Computed Tomography, Positron Emission Tomography.

Volume: 01 Issue: 02

Date of Publication: 2018-08-30

Journal: To physics Journal

Website: <https://purkh.com>



This work is licensed under a Creative Commons Attribution 4.0 International License.



Introduction

Between 1990 and 2015, liver cancer was the 6th most common cancer worldwide in terms of incidence and the 4th most common leading cause of mortality. In 2015 the global number of incident cases was estimated at 854.000, the number of deaths just slightly lower (810.000) [1]. The most prevalent type of primary liver cancer is hepatocellular carcinoma (HCC). Depending on the staging of HCC, several treatments including liver transplantation, hepatic resection, ablation, transhepatic artery chemoembolization (TACE) and radioembolization with yttrium-90 microspheres are available [2]. This article focuses on the latter.

The objective of the study was to assess the correspondence between the dose distribution calculated based on technetium-99m macroaggregated albumin (MAA) single photon emission computed tomography (SPECT) and yttrium-90 microspheres positron emission tomography (PET) based images, as well as the correspondence between the desired dose and the true dose in the target area.

Radioembolization with yttrium-90 microspheres

The first report of treatment of hepatic cancer with intraarterial infusion of yttrium-90 microspheres originates from the 1960s [3]. In the following decades, patients with HCC included in several studies were treated with yttrium-90 microspheres [4-6]. Triggered by the results of this palliative treatment an optimal radiation dose to the tumor was investigated, which was found to be > 120 Gy [7].

The amount of yttrium-90 activity needed to achieve the desired radiation dose can be calculated by the following formula (1).

$$A_{90Y} = \frac{D \cdot m_t}{C \cdot (1-F)} \quad (1)$$

With A_{90Y} the administered activity of yttrium-90 microspheres in GBq, D the desired dose to the target volume in Gy, m_t the mass of the target volume in kg and F the lung shunt fraction (LSF), the estimated amount of administered activity shunting to the lungs. The factor C in the denominator, with a value of 49.8 J GBq^{-1} , is a conversion factor reflecting the average deposited energy per GBq of administered yttrium-90 activity. It needs to be pointed out that (1) is a simplified view on reality, as it calculates the activity needed for a homogeneous dose distribution in a target volume with dimensions much larger than the yttrium-90 maximum beta range of approximately one centimeter in soft tissue.

Yttrium-90 decays almost exclusively (>99.9%) to zirconium-90 by emitting an electron with an average energy of 933.7 keV [8], but in addition 32 ppm of yttrium-90 decay yields emission of a positron [9]. Because of the different decay paths, the assessment of the distribution of yttrium-90 microspheres after administration can be done by performing either a SPECT/Computed Tomography (CT) scan or a PET/CT scan [10-11]. Using PET rather than bremsstrahlung SPECT for assessment of the yttrium-90 distribution provides images with higher image quality, because of the higher spatial resolution of PET imaging [12].

Dosimetry

When estimating the amount of yttrium-90 activity needed for radioembolization, a homogeneous radiation dose distribution in the target volume is assumed. The true dose distribution, however, depends on the distribution of the yttrium-90 microspheres in the liver, and may be of interest, as a relationship between tumor dose and response is suggested [13-16]. Real-time assessment of the distribution of yttrium-90 microspheres during administration is currently not feasible. Therefore, post-administration imaging is used to estimate the dose distribution.

To prevent the lungs from receiving an intolerable high dose, excessive shunting from the liver to the lungs or to the abdominal structures should be ruled out before treating a patient with yttrium-90 microspheres. Therefore, a scout dose technetium-99m MAA is administered two weeks before the yttrium-90 administration by infusion in the hepatic artery and subsequently imaged using Whole Body (WB) imaging on a SPECT/CT scanner. CT imaging can be appended to the study for both anatomical correlation and attenuation correction. The LSF can be estimated from the WB images.

Prospective dosimetry uses the technetium-99m MAA SPECT/CT scan as the expected distribution of yttrium-90 microspheres. Dose estimation can be performed by quantitative SPECT, evaluating the ratio of counts in different volumes of interest [17].



Patients with a low LSF are eligible for administration of yttrium-90 microspheres. The total lung dose must not exceed 30 Gy. Similar to technetium-99m MAA, administration takes place by infusion in the hepatic artery. Subsequently, the distribution of the microspheres can be assessed by PET/CT imaging. Acquired images can be used for patient specific retrospective dosimetry. As retrospective dosimetry is based on the true distribution of the microspheres, it will yield a reliable dose distribution when properly imaged. Phantom measurements showed that accurate dosimetry may be indeed provided using this method [10].

Methods

A. Selective internal radiation therapy (SIRT)

Five patients included in this retrospective study were treated with TheraSphere yttrium-90 glass microspheres (Nordion Inc., Ottawa, Canada) at the Department of Radiology & Nuclear Medicine at the VU University Medical Center, Amsterdam.

Patients with HCC were candidates for the procedure. The target volume was calculated by the radiologist through manual delineation of the contour on a diagnostic CT scan. For patients with multiple targets, multiple target volumes were retrieved. The mass of the target volume was obtained by multiplication of the target volume with the density of 1.03 g/ml. All administrations of both technetium-99m MAA and yttrium-90 microspheres were performed by the same experienced interventional radiologist under fluoroscopy (Philips Allura X FD20 (Philips Healthcare, Eindhoven, The Netherlands)) set to auto exposure. In each procedure, the catheter tip was positioned carefully to ensure technetium-99m MAA and yttrium-90 microspheres were administered from an identical position, see Figure 1.

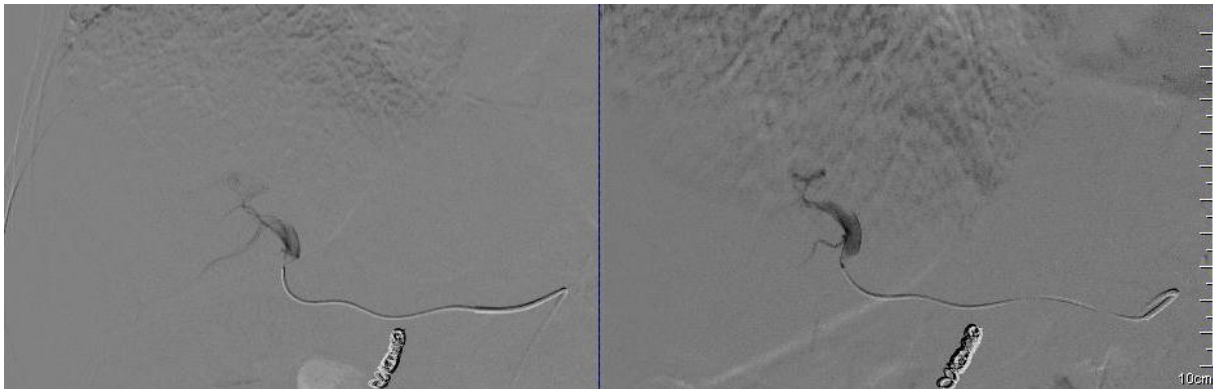


Figure 1 Identical placement of the catheter tip for administration of technetium-99m MAA (left) and yttrium-90 microspheres (right) two weeks after the administration of technetium-99m MAA. The coil in the lower mid part of both images, placed because of collateral vasculature nearby the tumor, is clearly visible and can be used as a reference.

Suitability for radioembolization with yttrium-90 microspheres was assessed for selected patients by performing a SPECT/CT scan. 100 MBq technetium-99m MAA was administered intravenously. 1 to 4 hours after administration, the patient was scanned using a dual-head Siemens Symbia T2 scanner, (Siemens AG, Erlangen, Germany).

Whole body imaging was performed from head to groin, with a bed speed of 12 cm/min, for on average 15 min. For the lung volume, a trapezium was used (as shown in Figure 2). The LSF was defined as the ratio between lung counts and whole body counts. A LSF of less than 5% was considered safe for yttrium-90 administration.

SPECT/CT data was acquired using a step and shoot method, covering 360 degrees in 32 steps of 40 seconds each. A standard technetium-99m energy window (129 – 150 keV) was used. For anatomical reference, a low dose CT scan with 5 mm slice thickness and 1.27 mm × 1.27 mm pixels was acquired.

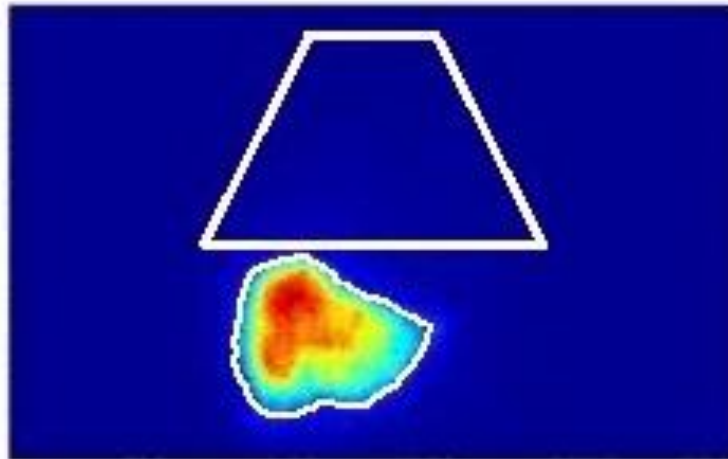


Figure 2 Definition of the lung ROI for evaluation of the LSF, shown in addition to the liver area. The liver is delineated using a threshold of 20% of the maximum number of counts per voxel.

Clinically used reconstructions were obtained using Filtered Back Projection (FBP). A generalized Hanning filter with cut-off set at 0.9 times the Nyquist frequency and a steepness factor of 0.5 was applied. Reconstructed slices had a thickness of 4.8 mm, and a pixel size of approximately $5 \times 5 \text{ mm}^2$. For the purpose of this study, an additional attenuation corrected iterative reconstruction was generated.

Similar to the technetium-99m MAA, the yttrium-90 microspheres were administered under fluoroscopy. Administered yttrium-90 activity ranged from 1.5 to 5.1 GBq. After administration, a PET/CT scan was acquired using a Philips Ingenuity TF PET/CT scanner (Philips Healthcare, Eindhoven, The Netherlands). Patients were scanned for 20 minutes (two bed positions of 10 minutes each). A helical low dose CT scan was performed for anatomical correlation and attenuation correction. Pixels of $1.17 \text{ mm} \times 1.17 \text{ mm}$ with a slice width of 5 mm were chosen. For the PET reconstructions, a method compliant with the EARL criteria [18] was used. The BLOB-OS-TF reconstruction algorithm without point spread function (PSF) modelling was performed [19]. Reconstructions were made using $4 \times 4 \times 4 \text{ mm}^3$ voxels and a 144×144 matrix, and in addition to CT-based attenuation correction, scatter correction and randoms correction was applied.

B. Computational

Assessment of the dose distribution inherent to the distribution of yttrium-90 microspheres was performed using the Geant4 Application for Tomographic Emission (GATE) [18]. GATE is an open source software package suitable for performing Monte Carlo based simulation, developed specifically for computations related to medical applications. Dose distributions were simulated using a geometry (the patient, represented by a CT scan), a source (the activity distribution in the patient, represented by a SPECT or PET scan) and a set of simulation parameters describing the behavior of emitted particles (the physics).

The types of tissue that an electron encounters on its path have impact on the location of deposition of its energy. In tissue with lower density, for example, an electron will lose less energy per unit length, and will therefore travel further. Using the CT scans acquired in SPECT/CT and PET/CT imaging, a patient-specific 3D map of material properties and atomic cross-sections was constructed. First, the Hounsfield Units (HU) were converted to different types of tissue using the method proposed by Schneider et al. [21]. Subsequently, the atomic compositions and density of these types of tissue were imported. For tissues that cover a large range of HU such as lung tissue, the compositions were specified in multiple intervals. The compositions were used to specify the cross sections.

To calculate the dose distribution based on the SPECT/CT scan, the assumption was made that the distribution of the technetium-99m MAA corresponds with the distribution of the yttrium-90 microspheres. As only a minor fraction of decays involves emitting a positron, the dose distribution can be closely approximated by only monitoring the emitted electrons. In



the simulation, $1 \cdot 10^7$ decay events are considered. The probability of a single event occurring in a voxel is linearly dependent on the number of counts in that voxel.

Each event leads to production of an electron with an initial energy E , which is also drawn from the probability distribution based on the energy spectrum [22]. Isotropic emission of electrons is assumed.

Regarding yttrium-90 as a pure beta-emitter, initially only electrons are produced. Interaction processes incorporated in the simulation include the photo-electric effect,

Compton and Rayleigh scattering, ionization and creation of bremsstrahlung. Secondary particles created in these processes are also tracked, and can contribute to the radiation dose. To avoid infrared divergence and thus limit computational costs, the secondary particles from electrons with an energy below 10 keV are not created. Deposited energy per voxel was monitored, and converted to radiation dose using the local density and voxel dimensions. To calculate the dose (as shown in Figure 3), the calculated radiation dose was scaled by the ratio between the total number of events in the patient N , calculated by equation (2), and the number of events considered in the Monte Carlo simulation.

$$N = A_0 \int_0^{\infty} e^{-\lambda t} dt \quad (2)$$

With A_0 the administered yttrium-90 activity and $\lambda = 3 \cdot 10^{-6} \text{ s}^{-1}$ [8] the decay constant. Due to the low positron yield, the PET images exhibited a high background level. Therefore, a background correction was applied. Additionally, both SPECT and PET dose images were smoothed by averaging each voxel with its neighbors (26-connectivity).

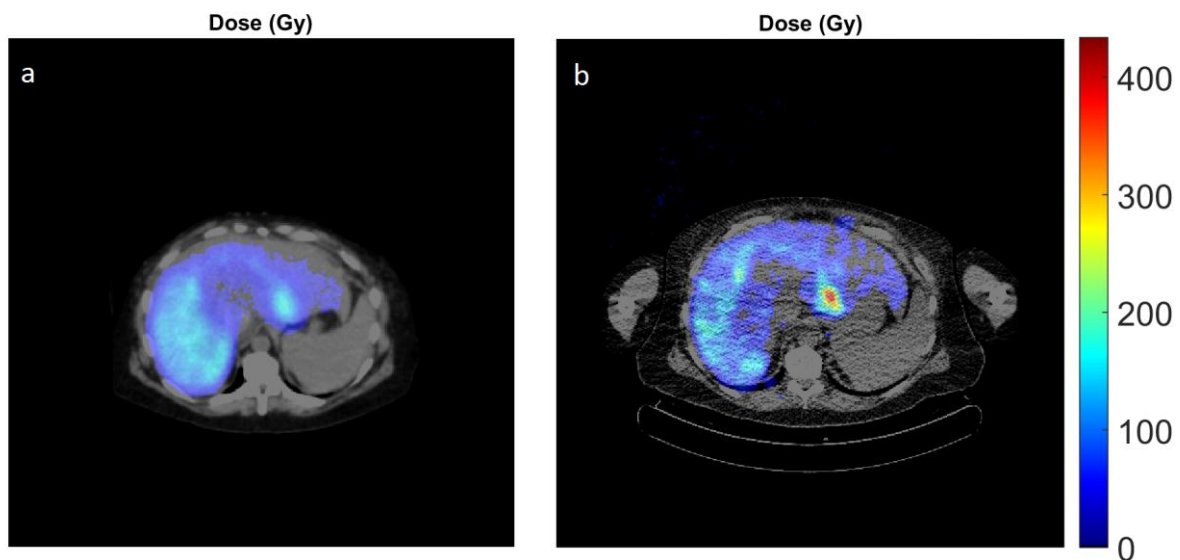


Figure 3 Visualization of the radiation dose distributions, calculated by Monte Carlo simulation based on technetium-99m MAA SPECT images (a) and yttrium-90 microspheres PET images (b). Notice that the PET-based dose distribution is less homogeneous, and also that the relative intensities in SPECT- and PET-based dose distributions are not similar.



Results

The dose distributions resulting from the technetium-99m MAA SPECT/CT scan and the yttrium-90 PET/CT scan were compared for each patient. Radiation dose profile characteristics were assessed (maximum local radiation dose, volume receiving a dose higher than a specified dose) and dose volume histograms (DVHs) were obtained.

Table 1 Maximum dose in a single voxel from dosimetry based on SPECT and PET imaging. Injected activity is determined by applying equation (1).

	Desired dose (Gy)	Yttrium-90 activity (GBq)	Target mass (kg)	'Rule of thumb' dose (Gy)	SPECT	PET
					Maximum dose (Gy)	Maximum dose (Gy)
Patient 1	120	3.78	1.483	127.4	786	294
Patient 2	100	2.29	1.099	104.2	383	243
Patient 3	120	8.34	3.197	130.5	209	434
Patient 4	120	3.80	1.547	123.7	345	237
Patient 5	120	4.42	1.773	125.0	451	374

Table 1 shows the parameters used for planning the procedure, as well as the maximum radiation dose calculated using the SPECT and PET images. The 'rule of thumb' dose is calculated under assumption of a homogeneous distribution of the administered yttrium-90 in the target volume. The maximum radiation dose shows differences between SPECT- and PET-based dosimetry ranging up to a factor two. The maximum radiation dose is larger than the 'rule of thumb' dose in all patients.



Table 2 Comparison of volumes receiving a radiation dose of at least the shown threshold value, determined by PET-based SPECT-based dosimetry.

Patient	Desired dose (Gy)	Target volume (cm ³)	Volume receiving a radiation dose (cm ³)							
			> 60 Gy		> 80 Gy		> 100 Gy		> 120 Gy	
			PET	SPECT	PET	SPECT	PET	SPECT	PET	SPECT
1	120	1339	877	720	502	601	314	516	192	448
2	100	1037	71	596	30	307	14	145	7	72
3	120	3016	2065	1750	1370	1135	850	788	486	402
4	120	1459	344	530	197	294	125	146	78	83
5	120	1673	493	1353	209	844	119	449	73	247

In Table 2 the volumes receiving a radiation dose above a threshold are indicated. The target volume was calculated from the target mass assuming the liver density used in the Monte Carlo simulations, $\rho_{liver} = 1.03 \text{ g/cm}^3$. Clearly, the volumes receiving a radiation dose of at least the desired dose are substantially smaller than the target volume indicated by the radiologist.

In four of five patients, the SPECT-based dose distribution yields a higher maximum dose than the PET-based dose distributions. Additionally, Figure 4 shows that in these four patients the SPECT-based volume receiving a certain dose is larger than or equal to the volume obtained from PET-based dose calculations for doses > 50Gy.

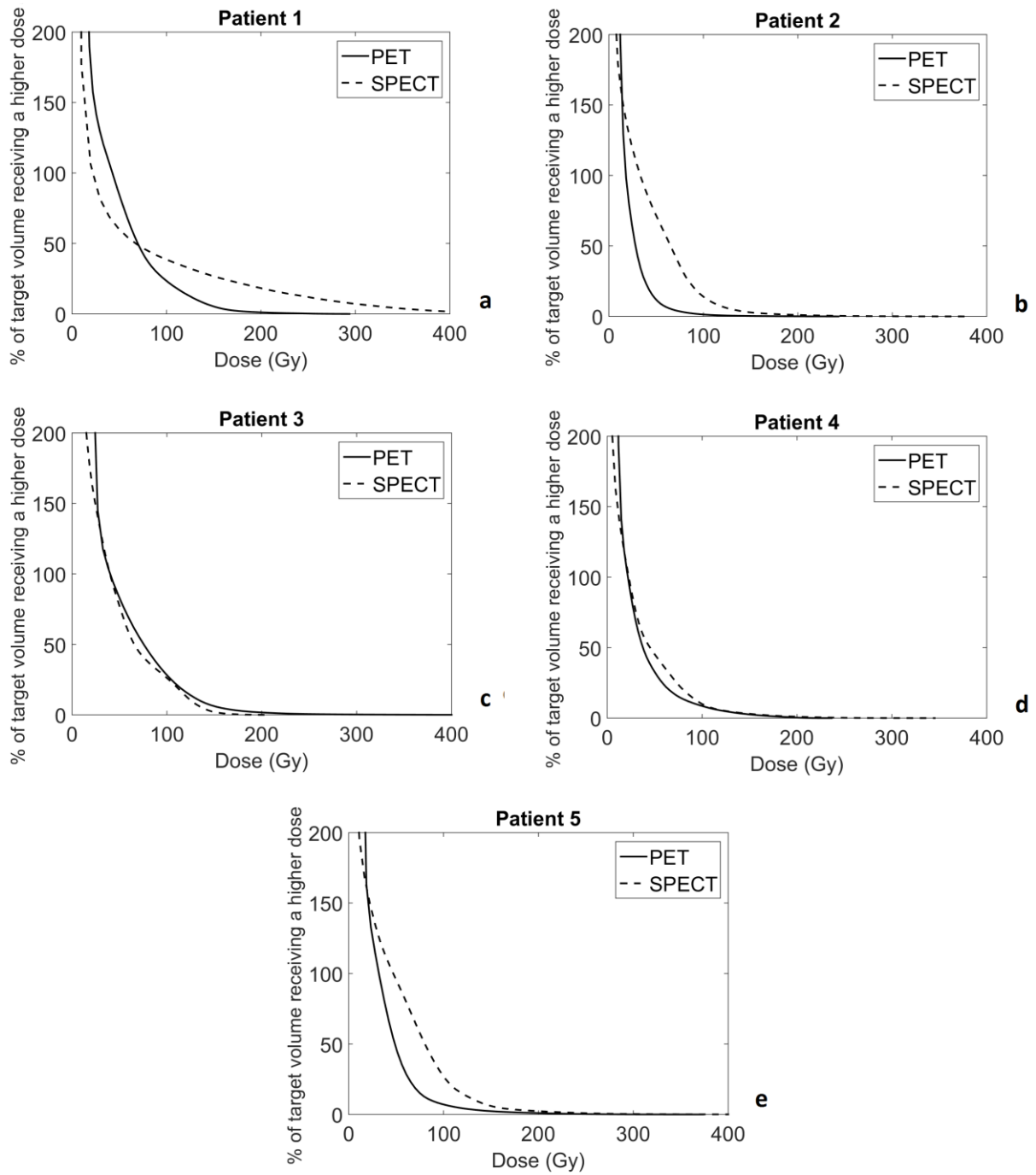


Figure 4 Dose volume histograms for patients 1 to 5 (a to e). The vertical axis shows the volume as a fraction of the total target volume, to correct for the differences in target volume.



Discussion

This study shows that dose distributions deduced from technetium-99m MAA SPECT do not necessarily mimic the dose distributions obtained from yttrium-90 microspheres PET.

Although patient benefits for yttrium-90 radioembolization are widely described in literature, improvements of pre-embolization dosimetry could lead to better tailored therapies. Patient specific treatment planning building on technetium-99m MAA SPECT-based dosimetry could contribute to better customization of treatments. The better the prediction is made using pre-embolization dosimetry, the better the estimate of the optimal injected activity. That way, damage to healthy liver tissue can be minimized.

A number of recent publications describe the feasibility of using technetium-99m MAA SPECT/CT for predictive dosimetry [15, 23-25]. More critical publications can also be found, mentioning significant differences comparing predictive SPECT-based and retrospective PET-based calculated absorbed doses in tumor and normal liver [26], poor correlation between yttrium-90 and technetium-99m MAA activity distributions [27], inaccurate prediction of the distribution of yttrium-90 [28] as well as overestimation [29] or underestimation [30] of tumorous uptake using predictive dosimetry. This is concordant with our results.

A recent study shows significant differences when comparing SPECT- and PET-based calculated absorbed doses in tumor and normal liver [26]. Other literature describes that technetium-99m MAA SPECT/CT-based dosimetry is accurate in HCC [23] and that predictive dosimetry is feasible for tumors [15]. In addition, Strigari et al. conclude that technetium-99m MAA SPECT images of the abdomen were sufficiently predictive of the yttrium-90 distribution in more than 90% of patients [25].

Only five patients were included in this study, therefore no quantitative relations between SPECT- and PET-based dosimetry were inferred from the obtained data. However, calculations carried out for these five patients suggest that pre-embolization dosimetry based on technetium-99m MAA SPECT imaging needs optimization before it can be reliably used in clinical practice for the treatment planning.

The background correction for PET data that was applied only induces a proportional increase in dose calculated based on the PET images. Therefore, it does not alter the shape of the dose volume histograms showed in Figure 4. Also, the PET-based calculated volume receiving a certain dose is smaller (4 patients) or similar (1 patient) after correction, which indicates that the applied correction leads to better correspondence between the two calculations.

Both PET- and SPECT-based calculated dose distributions were smoothed to decrease incidental maxima caused by count statistics. After smoothing SPECT-based dose distributions showed higher local maxima than the PET-based images. This difference can be attributed to the higher heterogeneity of the technetium-99m MAA distribution.

A large liver volume receiving a lower radiation dose than scheduled can result in inefficient or insufficient treatment, as a relation between tumor dose and response is suggested [13-16]. Because the volume receiving a dose above a certain threshold tends to be overestimated when relying on SPECT-based dosimetry, underdosing is a real possibility.

To better quantify the post-embolization dose distribution, PET images of a higher quality are required. With improvement of both pre- and post-treatment dosimetry, a better estimate of the dose response rate is expected. This can additionally be used to optimize the patient dose.

Conclusion

The inhomogeneity of the distribution of both technetium-99m MAA and yttrium-90 in the target volume results in a maximum local radiation dose that is higher than the average target radiation dose and the desired dose.

Since the relative technetium-99m MAA distribution does not necessarily comply with the distribution of yttrium-90 microspheres, technetium-99m MAA scans cannot be directly used for prospective radiation dose assessment.

**Data availability**

The datasets generated during and/or analyzed during the current study are not publicly available, but are available from the corresponding author on reasonable request.

Conflicts of Interest

Each author declares that he/she does not have conflicts of interest. This article does not contain any studies with human participants performed by any of the authors

Funding

This research did not receive any specific grant from funding agencies in the public, commercial, nor non-for-profit sectors.



References

- [1] Global Burden of Disease Cancer Collaboration. Global, regional, and national cancer incidence, mortality, years of life lost, years lived with disability, and disability-adjusted life-years for 32 cancer groups, 1990 to 2015: a systematic analysis for the global burden of disease study. *JAMA Oncol.* 2017;3(4):524–548. doi: [10.1001/jamaoncol.2016.5688](https://doi.org/10.1001/jamaoncol.2016.5688).
- [2] Schlachterman, A, Craft Jr, WW, Hilgenfeldt, E, Mitra, A, Cabrera, R. Current and future treatments for hepatocellular carcinoma. *World J Gastroenterol.* 2015;21(28):8478–8491. doi: [10.3748/wjg.v21.i28.8478](https://doi.org/10.3748/wjg.v21.i28.8478).
- [3] Simon, N, Feitelberg, S. Scanning brehmsstrahlung of Yttrium-90 microspheres injected intra-arterially. *Radiology.* 1967 Apr;88(4):719–24. doi: [10.1148/88.4.719](https://doi.org/10.1148/88.4.719).
- [4] Houle, S, Yip, TK, Shepherd, FA, et al. Hepatocellular carcinoma: pilot trial of treatment with Y-90 microspheres. *Radiology.* 1989 Sep;172(3):857–860. doi: [10.1148/radiology.172.3.2549567](https://doi.org/10.1148/radiology.172.3.2549567).
- [5] Blanchard, RJ, Morrow, IM, Sutherland, JB. Treatment of liver tumors with yttrium-90 microspheres alone; *Can Assoc Radiol J.* 1989 Aug;40(4):206–210
- [6] Herba, MJ, Illescas, FF, Thirlwell, MP, et al. Hepatic malignancies: improved treatment with intraarterial Y-90; *Radiology.* 1988 Nov;169(2):311–314 doi: [10.1148/radiology.169.2.3174978](https://doi.org/10.1148/radiology.169.2.3174978).
- [7] Lau, WY, Leung, WT, Ho, S, et al. Treatment of inoperable hepatocellular carcinoma with intrahepatic arterial yttrium-90 microspheres: a phase I and II study. *Br J Cancer.* 1994;70(5):994–999.
- [8] ENSDF Decay Data in the MIRD (Medical Internal Radiation Dose) Format for ⁹⁰Y
<https://www.orau.org/ptp/PTP%20Library/library/DOE/bnl/nuclidedata/MIRY90.htm>_Accessed 10 november, 2017
- [9] Nickles, RJ, Roberts, AD, Nye, JA, et al. Assaying and PET imaging of yttrium-90: $1 > 34\text{ppm} > 0$. *IEEE Symposium Conference Record Nuclear Science 2004., Rome, 2004*, pp. 3412–3414 vol. 6. doi: [10.1109/NSSMIC.2004.1466619](https://doi.org/10.1109/NSSMIC.2004.1466619).
- [10] Lhommel, R, van Elmbt, L, Goffette, P, et al. Feasibility of ⁹⁰Y TOF PET-based dosimetry in liver metastasis therapy using SIR-Spheres. *Eur J Nucl Med Mol Imaging.* 2010;37:1654–1662 doi: [10.1007/s00259-010-1470-9](https://doi.org/10.1007/s00259-010-1470-9).
- [11] Gates, VL, Esmail, AA, Marshall, K, Spies, S, Salem, R. Internal pair production of ⁹⁰Y permits hepatic localization of microspheres using routine PET: proof of concept; *J Nucl Med.* 2011 Jan;52(1):72–76. doi: [10.2967/jnumed.110.080986](https://doi.org/10.2967/jnumed.110.080986).
- [12] Elschot, M, Vermolen, BJ, Lam, MGEH, et al. Quantitative Comparison of PET and Bremsstrahlung SPECT for Imaging the In Vivo Yttrium-90 Microsphere Distribution after Liver Radioembolization. Villa E, ed. *PLoS ONE.* 2013;8(2):e55742. doi: [10.1371/journal.pone.0055742](https://doi.org/10.1371/journal.pone.0055742).
- [13] Garin, E, Rolland, Y, Pracht, M, et al. High impact of macroaggregated albumin-based tumour dose on response and overall survival in hepatocellular carcinoma patients treated with ⁹⁰Y-loaded glass microsphere radioembolization. *Liver Int.* 2017;37(1):101–110. doi: [10.1111/liv.13220](https://doi.org/10.1111/liv.13220).
- [14] Srinivas, SM, Natarajan, N, Kuroiwa, J, et al. Determination of radiation absorbed dose to primary liver tumors and normal liver tissue using post-radioembolization ⁹⁰Y PET. *Front Oncol.* 2014;4:255. doi: [10.3389/fonc.2014.00255](https://doi.org/10.3389/fonc.2014.00255).
- [15] Kao, Y-H, Steinberg, JD, Tay, Y-S, et al. Post-radioembolization yttrium-90 PET/CT – part 2: dose-response and tumor predictive dosimetry for resin microspheres. *EJNMMI Research.* 2013;3:57. doi: [10.1186/2191-219X-3-57](https://doi.org/10.1186/2191-219X-3-57).
- [17] Garin, E, Rolland, Y, Lenoir, L, et al. Utility of quantitative ^{99m}Tc-MAA SPECT/CT for ⁹⁰yttrium-labelled microsphere treatment planning: calculating vascularized hepatic volume and dosimetric approach. *Int J Mol Imaging.* 2011;2011:398051. doi: [10.1155/2011/398051](https://doi.org/10.1155/2011/398051).
- [18] Matej, S, Lewitt, RM. Practical considerations for 3-D image reconstruction using spherically symmetric volume elements. *IEEE Trans Med Imaging.* 1996;15(1):68–78. doi: [10.1109/42.481442](https://doi.org/10.1109/42.481442).



- [19] Boellaard, R, Delgado-Bolton, R, Oyen, WJG, et al. FDG PET/CT: EANM procedure guidelines for tumour imaging: version 2.0. *Eur J Nucl Med Mol Imaging*. 2015;42:328-354. doi: [10.1007/s00259-014-2961-x](https://doi.org/10.1007/s00259-014-2961-x).
- [20] Jan, S, Santin, G, Strul, D, et al. GATE - Geant4 Application for Tomographic Emission: a simulation toolkit for PET and SPECT. *Phys Med Biol*. 2004;49(19):4543-4561.
- [21] Schneider, W, Bortfeld, T, Schlegel, W, et al. Correlation between CT numbers and tissue parameters needed for Monte Carlo simulations of clinical dose distributions; *Phys Med Biol*. 2000 Feb;45(2):459-478.
- [22] Devaney, JJ. Beta spectra of ^{90}Sr and ^{90}Y . 1985;LA--10467-MS. United States
- [23] Garin, E, Rolland, Y, Laffont, S, Edeline, J. Clinical impact of $^{99\text{m}}\text{Tc}$ -MAA SPECT/CT-based dosimetry in the radioembolization of liver malignancies with ^{90}Y -loaded microspheres. *Eur J Nucl Med Mol Imaging*. 2016;43:559-575. doi: [10.1007/s00259-015-3157-8](https://doi.org/10.1007/s00259-015-3157-8).
- [24] Kao, YH, Hock Tan, AE, Burgmans, MC, et al. Image-guided personalized predictive dosimetry by artery-specific SPECT/CT partition modeling for safe and effective ^{90}Y radioembolization; *J Nucl Med*. 2012 Apr;53(4):559-566. doi: [10.2967/jnumed.111.097469](https://doi.org/10.2967/jnumed.111.097469)
- [25] Strigari, L, Sciuto, R, Rea, S, et al. Efficacy and toxicity related to treatment of hepatocellular carcinoma with ^{90}Y -SIR spheres: radiobiologic considerations; *J Nucl Med*. 2010 Sep;51(9):1377-1385. doi: [10.2967/jnumed.110.075861](https://doi.org/10.2967/jnumed.110.075861)
- [26] Song, YS, Paeng, JC, Kim, H-C, et al. PET/CT-Based Dosimetry in ^{90}Y -Microsphere Selective Internal Radiation Therapy: Single Cohort Comparison With Pretreatment Planning on $^{99\text{m}}\text{Tc}$ -MAA Imaging and Correlation With Treatment Efficacy. Zakko, S, ed. *Medicine*. 2015;94(23):e945. doi: [10.1097/MD.0000000000000945](https://doi.org/10.1097/MD.0000000000000945).
- [27] Knesaurek, K, Machac, J, Muzinic, M, et al.; Quantitative comparison of yttrium-90 (^{90}Y)-microspheres and technetium-99m ($^{99\text{m}}\text{Tc}$)-macroaggregated albumin SPECT images for planning ^{90}Y therapy of liver cancer; *Technol Cancer Res Treat*. 2010 Jun;9(3):253-262. doi: [10.1177/153303461000900304](https://doi.org/10.1177/153303461000900304)
- [28] Wondergem, M, Smits, ML, Elschot, M, et al.; $^{99\text{m}}\text{Tc}$ -macroaggregated albumin poorly predicts the intrahepatic distribution of ^{90}Y resin microspheres in hepatic radioembolization; *J Nucl Med*. 2013 Aug;54(8):1294-1301. doi: [10.2967/jnumed.112.117614](https://doi.org/10.2967/jnumed.112.117614)
- [29] Gnesin, S, Canetti, L, Adib, S, et al. Partition model-based $^{99\text{m}}\text{Tc}$ -MAA SPECT/CT predictive dosimetry compared with ^{90}Y TOF PET/CT posttreatment dosimetry in radioembolization of hepatocellular carcinoma: a quantitative agreement comparison; *J Nucl Med*. 2016 Nov;57(11):1672-1678; doi: [10.2967/jnumed.116.173104](https://doi.org/10.2967/jnumed.116.173104)
- [30] Rhee, S, Kim, S, Cho, J, et al. Semi-quantitative analysis of post-transarterial radioembolization ^{90}Y microsphere positron emission tomography combined with computed tomography (PET/CT) images in advanced liver malignancy: comparison with $^{99\text{m}}\text{Tc}$ macroaggregated albumin (MAA) single photon emission computed tomography (SPECT). *Nucl Med Mol Imaging*. 2016;50(1):63-69. doi: [10.1007/s13139-015-0366-9](https://doi.org/10.1007/s13139-015-0366-9).